Applied Energy 226 (2018) 797–807

Contents lists available at ScienceDirect

Applied Energy

journal homepage: www.elsevier.com/locate/apenergy

A solar methane reforming reactor design with enhanced efficiency

Jian Jin[a,b,1], Xin Wei[c,1], Mingkai Liu[a,b], Yuhang Yu[c], Wenjia Li[a,b], Hui Kong[a,b], Yong Hao[a,b,*]

[a] Institute of Engineering Thermophysics, Chinese Academy of Sciences, 11 Beisihuanxi Rd., Beijing 100190, PR China
[b] University of Chinese Academy of Sciences, No. 19A Yuquan Rd., Beijing 100049, PR China
[c] Department of Thermal Science and Energy Engineering, University of Science and Technology of China, Hefei, 230027, PR China

HIGHLIGHTS

- The thermal efficiency increases from 71% to 76.02% with the cutoff wavelength coating.
- The peak-to-mean flux ratio decreases from 5.42 to 3.07 with CPC device.
- The solar-to-chemical and thermal efficiency reach 59.16% and 76.02% at 850 °C and 1 atm.
- Methane conversion rate is 83.95% at temperature of 850 °C with Ni as catalyst.

ARTICLE INFO

Keywords:
Solar methane reforming
Thermochemical reactor
Cutoff wavelength coating
Compound parabolic concentrator
Efficiency

ABSTRACT

We report an efficiency-enhanced solar methane reforming reactor design, featuring cutoff wavelength coating over quartz window for incident solar energy, a compound parabolic concentrator (CPC) device for thermochemical performance enhancement and reticulated porous ceramics (RPC) structure of Ni/CeO_2-ZrO_2 used as the catalyst. A numerical model combining Monte-Carlo ray-tracing (MCRT) method with finite-element method (FEM) is established to evaluate the effectiveness of this reactor design. The simulation results show that the cutoff wavelength coating (with threshold wavelength of 2400 nm) helps to reduce 80% radiation heat loss from within the reactor at the cost of only 1% incident sunlight loss during transmission at a typical reforming temperature of 850 °C. The performance of the reactor is numerically investigated under different reaction conditions with wide ranges of temperature, solar power input and steam-to-methane ratio. Results show that $\eta_{solar-chemical}$ (solar-to-chemical efficiency) can reach 39.98% and 59.16% without and with 90% heat recovery, respectively, and X_{CH_4} (methane conversion) is 83.95% at reforming temperature of 850 °C and pressure of 1 atm. The new reactor design could considerably increase the utilization efficiency of solar energy.

1. Introduction

The sun is an enormous source of sustainable and clean energy. The annual amount of incident solar energy on the earth considerably exceeds the world's energy demand [1]. However, solar energy is difficult to capture and utilize in an efficient manner due to its low density, intermittency and limited energy conversion efficiency. One approach of solar energy utilization is the conversion of solar energy into chemical energy by means of solar thermochemical processes. This approach has the advantages of relatively high energy conversion efficiency, as well as easy storage and transportation of solar energy [2]. As one of those promising technologies that use concentrated solar energy to convert primary fossil fuels into syngas (a mixture of H_2 and CO) [3], solar methane reforming is a potentially more effective approach of solar energy utilization compared with single-form (i.e. solar-only) solar thermal or photovoltaic technologies. The solar syngas thus derived also provides an ideal feedstock for industrial processes (such as the Fischer-Tropsch synthesis [4]) for further synthesis of liquid fuels. Besides the apparent advantages of solar energy being plentiful and methane being widely used as one of the primary energy sources, solar methane reforming remains a promising research direction for at least two reasons: (1) significant conversion rates could be achieved at relatively low temperatures compared with many other solar thermochemical systems (e.g. solar cracking); (2) thermal energy for driving the reforming reaction is provided by concentrating the entire solar spectrum, which saves a considerable fraction (i.e. 30%) of methane that otherwise has to be combusted to supply the required heat in industry [5]. The calorific value of syngas is 23.1% and 27.7% higher

* Corresponding author at: Institute of Engineering Thermophysics, Chinese Academy of Sciences, 11 Beisihuanxi Rd., Beijing 100190, PR China.
E-mail address: haoyong@iet.cn (Y. Hao).
[1] Equal-contribution first authors.

https://doi.org/10.1016/j.apenergy.2018.04.098
Received 9 January 2018; Received in revised form 10 April 2018; Accepted 28 April 2018
Available online 14 June 2018
0306-2619/

than that of the input methane, converted through steam methane reforming (SMR) and CO_2 methane reforming (CMR) routes, respectively [6].

$$SMR: CH_4 + H_2O \rightleftharpoons CO + 3H_2,\ \Delta H^{\ominus}_{298K} = +206.1\ kJ/mol \quad (1)$$

$$CMR: CH_4 + CO_2 \rightleftharpoons 2CO + 2H_2,\ \Delta H^{\ominus}_{298K} = +247.3\ kJ/mol \quad (2)$$

Compared with CMR, SMR has its unique advantages: (1) it produces syngas with the highest H_2-to-CO ratio (a primary way for industrial hydrogen production); (2) higher conversion rates of methane could be obtained due to the lower equilibrium temperature of SMR than that of CMR; (3) carbon deposition, causing catalyst deactivation, is less severe than that of CMR, which can be explained in two aspects. One is that due to lower operating temperatures, carbon deposition caused by deep cracking of methane [7,8] thermodynamically favored at high temperatures [9], can be avoided, and the other is that carbon deposition is less favored at lower C/H ratios. Hence catalyst for SMR might have a considerably longer life and better catalytic effect.

Studies on solar methane reforming in the literature mainly involve analyses on thermodynamics and kinetics [10,11], catalysts [12–14], reactor design [15] and system [16]. Although theoretical methane conversion can reach nearly 100% at 850 °C and 1 atm (CH_4:H_2O = 1:2), which is calculated by minimizing the Gibbs free energy of system, actual methane conversion is usually kinetically limited, so that catalysts are needed to enhance reaction rates. Active catalyst is loaded on the surface of certain supports such as Al_2O_3, ZrO_2, CeO_2-ZrO_2 [17,18], which is typically fabricated into a porous structure to maximize the surface area of dispersed catalyst particles in order to enhance chemical reaction rates.

The process inside the reactor is a complex one coupling absorption of concentrated sunlight, heat transfer (radiation, heat conduction and convection), mass transfer and chemical reactions. An effective high-temperature solar thermochemical reactor is key to converting solar energy into chemical energy via solar methane reforming. Solar methane reforming reactors can be classified as indirect and direct types [19]. Indirect reactors need a working medium to transfer solar heat to the reaction zone, the system design of which is more complex, and suitable heat transfer media are difficult to find at typical solar methane reforming temperatures. Direct reactors are directly exposed to concentrated solar radiation, which usually consists of three parts: a quartz window that sunlight can penetrate while reaction gas is isolated from the ambient; a catalyst bed absorbing solar energy and accelerating reactions; a well-designed thermal insulation wall reducing heat loss. Due to their simple design and flexible operation, direct reactors are the mainstream type among solar methane reforming reactors.

Several types of direct solar methane reforming reactor have been proposed and investigated [20–23]. The influence of solar flux distribution [24], reactants flow rate [25] and steam-to-methane ratio [26] on methane conversion and solar-to-chemical efficiency was analyzed. It was generally reported in the literature that methane conversion continuously rose with increasing reaction temperature [27], and that uniform heating of the catalyst bed by direct concentrated sunlight was crucial [28]. However, the radiation flux of concentrated sunlight exhibits Gaussian-like distribution, causing non-uniform solar flux distribution (and thus temperature non-uniformity) in the catalyst bed. Moreover, the thermal conductivity of catalyst support (foam structure of metal oxides) is usually not high enough to conduct heat to catalyst surfaces in a timely manner. As a result, hot spots and large temperature gradients often exist in the catalyst bed, which has tremendous impacts on the operation of reforming reactors, such as inducing undesired side reactions, catalyst degradation and thermal stress [29]. Therefore, enhancing the temperature distribution uniformity of catalyst bed is particularly important. This objective can be achieved in two possible ways: one is by homogenizing the solar flux distribution inside the cavity, and the other is by improving the radiation absorption and heat transfer characteristics of catalyst bed. As for the former solution, a compound parabolic concentrator (CPC) device has the function of homogenizing flux density [30], which is usually used for solar thermal applications [31], such as solar thermochemical reactors [32]. In addition, optimizing the shape of catalyst bed to match the solar flux distribution can also reduce the non-uniformity of the latter. For the second approach, an effective measure with a dual-scale porosity structure, namely reticulated porous ceramics (RPC) [33], could be employed for volumetric absorption of the solar flux by the catalyst bed. With those measures, the non-uniformity of temperature distribution could be greatly alleviated.

A good solar methane reforming reactor shall be capable of achieving not only high methane conversion but also high solar energy utilization efficiency (solar-to-chemical efficiency and thermal efficiency), which is vital for reactor design. Meanwhile, improving the efficiency of solar energy utilization can reduce the area of mirrors for solar energy collection, so that the overall system could be more cost-effective and flexible. Among major factors affecting solar energy utilization efficiency, heat loss via conduction (and subsequent convection) can be reduced by enhancing insulation, while heat loss via thermal radiation is much harder to reduce. In the typical methane reforming temperature range of 750–950 °C, thermal radiation loss from the reactor becomes predominant among all forms of heat loss. An effective way to decrease radiation heat loss is covering the quartz window with cutoff wavelength coating, which allows wavelengths shorter than a threshold value (i.e. the cutoff threshold) to go through and simultaneously reflects wavelengths longer than the threshold value almost totally [34]. A common example is the selective coating on the absorber tube wall of parabolic trough solar collectors, which has high absorptivity and low emissivity [35]. In the same rationale, a spectral selective coating could also be applied to the quartz window of a cavity-type solar collector/reactor, which transmits most of solar radiation and reflects the majority of thermal radiation back to the reactor cavity. However, a key difference is that the coating over a trough collector is absorptive for the purpose of sunlight-to-heat conversion, while that over a quartz window shall be transmissive to the majority part of the solar spectrum, with sunlight-to-heat conversion accomplished by the cavity instead. Consequently, thermal radiation loss might be greatly reduced, and temperature of quartz window could also be reduced since the majority fraction of radiation emitted by the cavity is reflected back. Röger et al. [36] proposed an ideal cutoff wavelength coating which reflects the long-wavelength part of a blackbody radiation spectrum ($\lambda > 2500$ nm) back into reactor without noticeably reducing the transmittance of solar spectrum. Their simulation results showed that a quartz window with coating can reduce 11% in receiver loss compared with an uncoated window at the temperature of 1100 °C. This technology is mainly based on the different spectral distribution between sunlight and blackbody radiation from the interior of a thermal reactor, and has the ability of reflecting most (e.g. ~80% at 850 °C) of thermal radiation back into reactor at the cost of a small fraction of incident solar energy loss (i.e. 1% at wavelength of 2400 nm). Meanwhile, the device of CPC also has the function of reducing thermal radiation loss due to the reduction of aperture diameter [37].

In this paper, a solar methane reforming reactor concept featuring cutoff wavelength coating, CPC device and RPC structure of Ni/CeO_2-ZrO_2 catalyst is proposed for solar methane reforming, which could improve methane conversion and efficiency of solar energy utilization. Major design principles of the reactor include reducing heat losses and improving uniformity of temperature distribution within catalyst bed. Correspondingly, cutoff wavelength coating, CPC device [31] and reticulated porous ceramics (RPC) structure [38] of catalyst are employed in this work to such ends. In the literature, solar thermochemical reactors for temperature-swing splitting of water or CO_2 at very high temperatures (e.g. 1600 °C) were the first to adopt the designs of CPC and RPC. In Ref. [32], a CPC device is used to further increase the solar concentration ratio and reduce thermal radiation loss by shrinking the

diameter of the aperture. In Refs. [33] and [38], a dual-scale RPC was proposed and used in a thermochemical reactor, which proved effective in promoting deeper penetration and volumetric absorption of sunlight, also resulting in a higher specific surface area of the catalyst bed. A key difference between the application of CPC in a thermochemical water/CO_2 splitting reactor and that in a methane reforming reactor lies in the fact that the operating conditions of the latter are much more benign. That is, not only the temperature is significantly lower (750–950 °C instead of 1450–1650 °C), but the atmosphere remains reducing (while that of the former alternates between oxidizing and reducing). Such conditions are benificial to protecting the CPC, which is usually metal-textured with a highly reflective surface, and thus could relieve or even eliminate its cooling burden. Meanwhile, as far as the authors are aware of, cutoff wavelength coating has not been previously employed in solar methane reforming reactors either. This signifies the possibility of further reduction of thermal radiation loss to the ambient and thus of achieving considerably enhanced efficiency via improved reactor design.

Thermodynamic and kinetic analyses are presented to illustrate the design principles of this reactor. A combination of Monte-Carlo ray-tracing (MCRT) method with finite-element method (FEM) is applied to evaluate the performance of the solar methane reforming reactor, taking kinetics of catalyst into consideration. Effects of solar power input and steam-to-methane ratio on methane conversion and solar-to-chemical efficiency are numerically investigated, and the results show significance in guiding the design of efficient solar methane reforming reactors.

2. Modeling of solar methane reforming reactor

2.1. Physical model

A conceptual solar methane reforming system, consisting of a parabolic solar dish collector and a cavity receiver/reactor, is illustrated in Fig. 1(a). The dish collector focuses sunlight with a concentration ratio of ~880, and then the concentrated sunlight, after going through the quartz window, is further converged by the CPC and eventually enters the cavity to drive the reforming reaction. Parameters of the reflector (i.e. solar dish collector) are summarized in Table 1.

The reactor, heated directly by focused solar beam for achieving high volumetric reaction rates, is illustrated in Fig. 1(b). The reactor consists of several parts: a quartz window of 120 mm in diameter and 5 mm in thickness with cutoff wavelength coating; cooling channel is placed in the upper part of the reactor for carrying residual heat away; CPC has an acceptance half angle of 45° and diameters of front and near apertures of 50 mm and 35.2 mm, respectively. An RPC structure [38] of CeO_2-ZrO_2 loaded with Ni catalyst [17] is placed in the reaction zone as the catalyst bed. The shape of catalyst bed is a hemispherical shell with inner and outer diameters of 110 mm and 160 mm, respectively. For the purpose of minimizing convective heat loss to the ambient, the reactor employs an insulation design to cut down heat conduction with a conductivity coefficient of 0.25 $W\,m^{-1}\,K^{-1}$ of the wall (Al_2O_3, with a thickness of 120 mm). The shell of reactor is made of stainless steel. Hence, this reactor can also stand relatively high pressures (i.e. 5 atm), while the influence of pressure on solar steam methane reforming will be studied in future. The present work mainly emphasizes studies on the design and operation of methane reforming reactors with the features of cutoff wavelength coating, CPC and RPC. Therefore, the temperature and pressure inside the cavity reactor are taken as ~850 °C and 1 atm, respectively. The total incident solar power of the system is set to 2.0 kW, and main operating parameters of reactor are shown in Table 2.

Table 1
Operating parameters of the parabolic dish collector.

Parameters	Value
Diameter of parabolic dish collector	1.596 m
Focal length	0.963 m
Solar collector optical efficiency	0.93
Specular error	2 mrad
Solar irradiance	1 kW/m^2

The cutoff wavelength coating allows shorter wavelengths to go through and simultaneously reflects longer wavelengths for different spectral energy distributions of sunlight and thermal radiation from within the cavity (by Planck's law). With the help of the coating, most of radiation from within the reactor is reflected back to the cavity, and the reflected radiation partially returns to the reaction zone through CPC aperture; the other part is absorbed by the inner surface of the cone to preheat the reactants.

However, application of the cutoff wavelength coating might also reduce the sunlight transmittance of the quartz window. Consequently, whether the coating is beneficial to the reactor's performance depends on the real transmittance of the quartz window integrated with the coating. Ref. [36] analyzed different kinds of coatings with cutoff wavelength of 2500 nm and showed that receiver loss could be reduced by 11% at 1100 °C. Then a 25 μm-thick coating was made and the result of

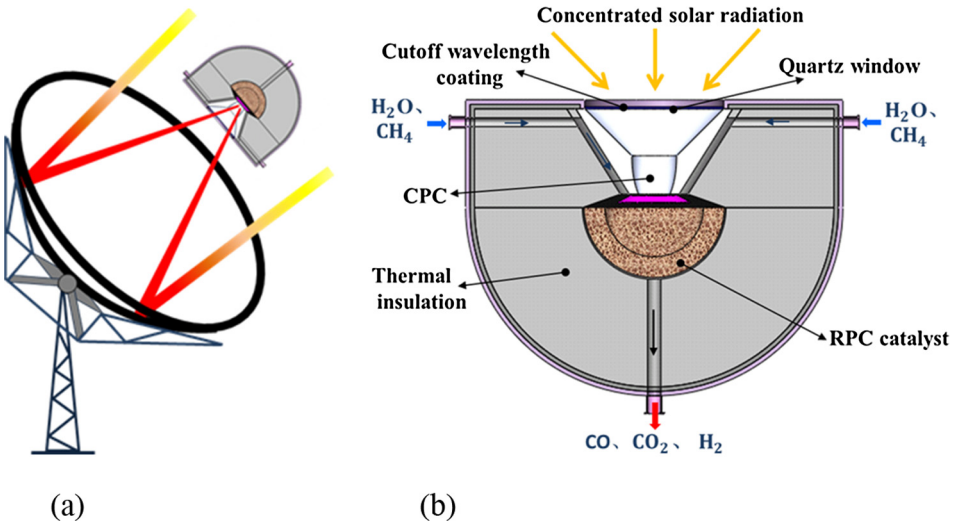

Fig. 1. (a) Schematic of a solar methane reforming device with a parabolic dish collector; (b) Schematic of a solar methane reforming reactor for the production of syngas, with a thermally insulated cavity receiver containing porous monolithic catalyst.

Table 2
Operating parameters of the reactor.

Parameters	Value
Temperature of the reactor	~850 °C
Pressure of the reactor	1 atm
Ratio of H_2O/CH_4	2
Flow rate of CH_4	0.005 mol/s
Diameter of quartz window	120 mm
Thickness of quartz window	5 mm
Transmittance of quartz window	0.95
Upper aperture diameter of CPC	50 mm
Acceptance half-angle of CPC	45°
Inner diameter of catalyst	110 mm
Thickness of catalyst	25 mm
Porosity of catalyst	76%

spectral measurement fitted satisfactorily to the design value.

The CPC is employed for two major purposes: one is to further boost solar concentration ratio and reduce radiation loss; the other is to enhance uniformity of solar energy distribution within the cavity, thereby minimizing temperature gradient.

Methane reforming catalyst is assumed to be Ni/CeO_2-ZrO_2 [17]. The catalyst carrier is made of ceria and zirconia with an RPC structure, and then Ni is loaded onto the surface. The RPC structure has been applied to high-temperature solar-driven H_2O/CO_2 splitting reactors for efficient solar energy absorption [33]. The RPC has dual-scale pores with mm-sized ones for enhancing heat and mass transport and μm-sized ones for enhancing the surface area of catalyst for better kinetics [39].

2.2. System description

Key reactions of steam methane reforming include Eq. (1) and the following equations [40]:

$$CO + H_2O \rightleftharpoons CO_2 + H_2,\ \Delta H^{\ominus}_{298K} = -41.2\ \text{kJ/mol} \quad (3)$$

$$CH_4 + 2H_2O \rightleftharpoons CO_2 + 4H_2,\ \Delta H^{\ominus}_{298\,K} = 164.9\text{kJ/mol} \quad (4)$$

Fig. 2 shows the schematic of the solar steam methane reforming system studied, which consists of a feed section and a reaction section. In the feed section, water is heated to 102 °C by solar energy with the purpose of mixing steam with methane and avoiding vaporization of water inside the reactor. The flow rate of steam is controlled by a constant-flow pump. It should be pointed out that the reactants can also be heated up by recuperating waste heat of products. Finally, the mixture of steam and methane flows into the reactor where reforming reaction takes place, and syngas is produced in the reaction section.

2.3. Modeling and simulation methodology

Physical and chemical processes of reactants preheating and steam methane reforming under steady state are simulated by Aspen Plus [41]. The flow field, temperature field and species distribution within the reactor are modeled and analyzed by the FEM method in combination with MCRT. The MCRT method is employed to optimize the geometry of the reactor and calculate solar energy flux distribution over the inner surface of the catalyst bed.

3. Analytical methodology

3.1. Concentrated solar flux on the solar reactor

Solar energy flux profile arriving at the reactor is calculated by the MCRT method. The number of rays is set to 5×10^7, which is accurate enough for the model [42]. To achieve a more realistic simulation of sunlight concentration process, the shape of the sun and the characteristics of cutoff wavelength coating are taken into account, and solar energy flux is set as thermal boundary condition for the FEM model.

3.2. Governing equations and boundary conditions

An FEM model is proposed to solve the coupled physical and chemical processes in this study, including the flow, heat transfer (conduction, convection, radiation), and chemical reactions.

3.2.1. Flow field analysis

Steam and methane are mixed and then fed into the cavity reactor. The mixture flows through the interlayer of cone and are heated by the radiation reflected by the cutoff wavelength coating. The mixed reactants that flow through the catalyst bed from inside to outside are converted into syngas within the catalyst bed.

The catalyst is approximated as a homogeneous continuum with specified parameters of porous media for the convenience of simulation. The flow inside the cavity reactor is single-phase laminar flow owing to the low Reynolds number (Re < 350). The governing equations are given as follows.

The steady-state continuity equation is given as:

$$\nabla\cdot(\rho\vec{u}) = 0 \quad (5)$$

where ρ and $\vec{u}$ represent the density and velocity of gas mixture, respectively.

The steady-state momentum equation of flow inside the cavity reactor is:

$$\frac{\nabla\cdot(\rho\vec{u}\vec{u})}{\varepsilon_p^2} = \nabla\cdot\left[-P\vec{I} + \frac{\mu}{\varepsilon_p}(\nabla\vec{u} + (\nabla\vec{u})^T) - \frac{2\mu}{3\varepsilon_p}(\nabla\cdot\vec{u})\vec{I}\right] - \mu\kappa^{-1}\vec{u} \quad (6)$$

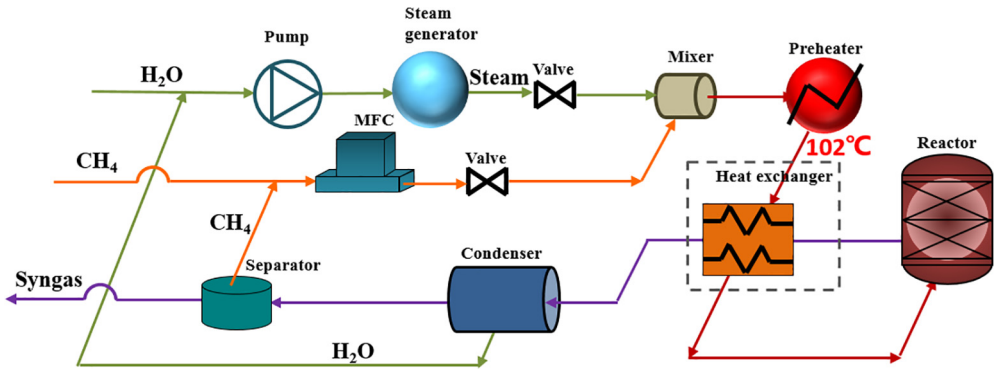

Fig. 2. Schematic of the solar steam methane reforming system studied in this work.

where ε_p is the porosity of the catalyst bed, P and μ are the pressure and the dynamic viscosity of reactants, respectively; permeability of catalyst bed κ is described by [43]:

$$\kappa = \frac{d_p^2 \varepsilon_p^3}{150(1-\varepsilon_p)^2} \tag{7}$$

where d_p represents the equivalent diameter of catalyst particles.

3.2.2. Thermal analysis

The concentrated solar radiation flux simulated by the MCRT method is volumetrically absorbed by the RPC catalyst first and then converted to heat for driving chemical reactions at ~850 °C, with heat losses resulting from heat convention and radiation.

The steady-state energy equation can be expressed as follows, assuming no body forces or viscous dissipation with concentrated solar radiation severing as thermal boundary condition:

$$\rho C_p \vec{u} \cdot \nabla T = \nabla \cdot (\lambda_{\text{eff}} \nabla T) + \dot{q} \tag{8}$$

where the effective thermal conductivity of the reaction zone is expressed as:

$$\lambda_{\text{eff}} = \theta_p \lambda_p + (1-\theta_p)\lambda \tag{9}$$

where C_p and T represent the specific heat and temperature of reactants, respectively; $\dot{q}$ denotes heat flux, including thermal and chemical components; λ_p and θ_p represent thermal conductivity and volume fraction of the catalyst, respectively; λ is the thermal conductivity of the gas mixture.

The boundary condition at the inner surface of the catalyst bed is given as:

$$-\lambda \left(\frac{\partial T}{\partial n}\right)_{n.a} + \sigma \varepsilon_s X_{1,2}(T_1^4 - T_2^4) + h\Delta T_1 = \dot{q} \tag{10}$$

where ε_s is the emissivity of the inner surface, expressed by:

$$\varepsilon_s = \frac{1}{1 + X_{1,2}(1/\varepsilon_1 - 1) + X_{2,1}(1/\varepsilon_2 - 1)} \tag{11}$$

where σ stands for Stefan-Boltzmann constant; $X_{1,2}$ and $X_{2,1}$ are the view factor of two surfaces (inner surface of the catalyst bed and inner surface of the reactor); ε_1 and ε_2 represent the emissivity of the two surfaces; h is the coefficient of convective heat transfer; ΔT_1 is the temperature difference between the inner surface of the catalyst bed and reactants; T_1 and T_2 are the temperatures of the two surfaces. The boundary condition at the outer surface of the cavity reactor is given as:

$$-\lambda \left(\frac{\partial T}{\partial n}\right)_{n.b} = h\Delta T_2 + \sigma \varepsilon_3 (T_3^4 - T_4^4) \tag{12}$$

where ΔT_2 is the temperature difference between the outer surface of the reactor and the ambient; ε_3 is the emissivity of the outer surface; T_3 and T_4 are the temperatures of the outer surface and the ambient, respectively.

3.2.3. Species conservation analysis

Ni supported by an RPC structure made of ceria-zirconia [17] is used as the catalyst in this study. Parameters of the reactor in this numerical model are shown in Table 2. The mass conservation equation for gas-phase species i, including Fick diffusion and convection, is given as:

$$\nabla \cdot \left(-\rho_i D_i \nabla \omega_i - \rho_i \omega_i D_i \frac{\nabla M_n}{M_n}\right) + \rho_i (\vec{u} \cdot \nabla)\omega_i = R_i \tag{13}$$

where R_i is the reaction rate of the gas componentspecies i, expressed by:

$$R_i = \sum_{j=1}^{3} \sigma_{ij} N_i r_j \tag{14}$$

Table 3
Stoichiometric coefficients of gas-phase species in chemical reactions.

σ_{ij}		i				
		1	2	3	4	5
j	1	−1	−1	+3	+1	0
	2	0	−1	+1	−1	+1
	3	−1	−2	+4	0	+1

where ω_i is the mass fraction of gas-phase species i (i = 1, 2, 3, 4 and 5, corresponding to CH_4, H_2O, H_2, CO and CO_2, respectively); M_n represents the average molar mass of gas mixture; N_i represents the molar mass of the gas species i; r_j denotes global reaction rate of reaction j (j = 1, 2 and 3, corresponding to Eqs. (1), (3) and (4)); D_i is binary diffusion coefficient of species i from the Fuller-Schettler-Giddings theory [44]; σ_{ij} is stoichiometric coefficient of gas-phase species i of reaction j, shown in Table 3.

For simplicity of analysis, only the three reactions, i.e. Eqs. (1), (3) and (4) are considered to take place in the reactor. Their reaction rates are expressed as follows according to Ref. [45].

$$r_1 = \frac{k_1/P_{H_2}^{2.5}(P_{CH_4}P_{H_2O} - P_{H_2}^3 P_{CO}/K_{eq,1})}{\text{DEN}^2} \tag{15}$$

$$r_2 = \frac{k_2/P_{H_2}(P_{CO}P_{H_2O} - P_{H_2}P_{CO_2}/K_{eq,2})}{\text{DEN}^2} \tag{16}$$

$$r_3 = \frac{k_3/P_{H_2}^{3.5}(P_{CH_4}P_{H_2O}^2 - P_{H_2}^4 P_{CO_2}/K_{eq,3})}{\text{DEN}^2} \tag{17}$$

$$\text{DEN} = 1 + K_{H_2}P_{H_2} + K_{CH_4}P_{CH_4} + K_{CO}P_{CO} + K_{H_2O}\frac{P_{H_2O}}{P_{H_2}} \tag{18}$$

where k_j is reaction rate constant of reaction j; K_i is adsorption constant of chemical species i; $K_{eq,j}$ is thermodynamic equilibrium constant of reaction j; P_i is the partial pressure of chemical species i. The specific expressions of such kinetic parameters are shown in Table 4.

3.3. Thermodynamic performance criteria of the system

In this study, the performance metrics of the solar methane reforming reactor, including (i) thermal efficiency, (ii) solar-to-chemical efficiency, and (iii) methane conversion, are investigated within a wide range of solar power input and steam-to-methane ratio conditions.

Thermal efficiency is defined as the fraction of solar energy converted to and utilized as thermal energy [46]:

Table 4
Kinetic parameters of Ni-based catalyst for steam methane reforming [40].

Parameters	Expression	Unit
k_1	$3.711 \times 10^{17} e^{\frac{-2.401 \cdot 10^5\ \text{J/mol}}{RT}}$	(mol $Pa^{0.5}$ kg_{cat}^{-1} s)
k_2	$5.431 e^{\frac{-6.713 \cdot 10^4\ \text{J/mol}}{RT}}$	(mol Pa^{-1} kg_{cat}^{-1} s)
k_3	$8.960 \times 10^{16} e^{\frac{-2.439 \cdot 10^5\ \text{J/mol}}{RT}}$	(mol $Pa^{0.5}$ kg_{cat}^{-1} s)
K_{H_2}	$6.12 \times 10^{-14} e^{\frac{8.29 \cdot 10^4\ \text{J/mol}}{RT}}$	Pa^{-1}
K_{CH_4}	$6.65 \times 10^{-9} e^{\frac{3.828 \cdot 10^4\ \text{J/mol}}{RT}}$	Pa^{-1}
K_{CO}	$8.23 \times 10^{-10} e^{\frac{7.065 \cdot 10^4\ \text{J/mol}}{RT}}$	Pa^{-1}
K_{H_2O}	$1.77 \times 10^5 e^{\frac{-8.868 \cdot 10^4\ \text{J/mol}}{RT}}$	1
$K_{eq,1}$	$1.198 \times 10^{23} e^{\frac{-26830\ \text{K}}{T}}$	Pa^2
$K_{eq,2}$	$1.\ 767 \times 10^{-2} e^{\frac{4400\ \text{K}}{T}}$	1
$K_{eq,3}$	$K_{eq,1}K_{eq,2}$	Pa^2

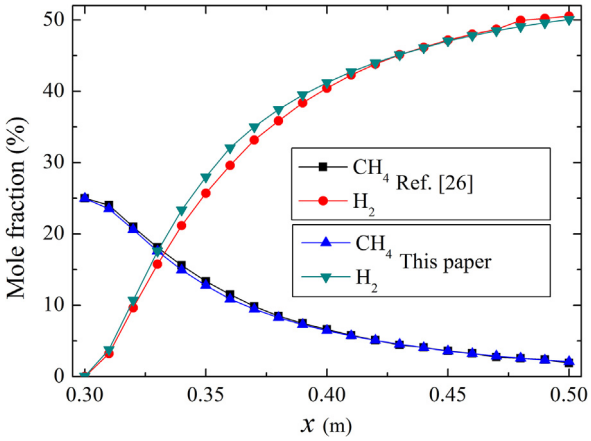

Fig. 3. Molar fractions of methane and hydrogen along the flow direction between results of experimental study Ref. [26] and numerical simulation study in this work.

$$\eta_{\text{thermal}} = 1-\frac{\dot{Q}_{\text{loss}}}{\dot{Q}_{\text{solar}}} = 1-\frac{\dot{Q}_{\text{con,loss}} + \dot{Q}_{\text{rad,loss}}}{\dot{Q}_{\text{reactor}} + \dot{Q}_{\text{preheater}}} \tag{19}$$

where $\dot{Q}_{\text{loss}}$ is the heat loss rate of the reactor, which is the sum of heat convention loss ($\dot{Q}_{\text{con,loss}}$) and thermal radiation loss ($\dot{Q}_{\text{rad,loss}}$). $\dot{Q}_{\text{solar}}$ is the solar power input, which consists of two parts: $\dot{Q}_{\text{preheater}}$ is the solar power used to heat reactants from 25 °C to 102 °C, and $\dot{Q}_{\text{reactor}}$ is the solar power gathered by the parabolic dish concentrator and used to drive the reactions.

Solar-to-chemical efficiency is defined as the fraction of solar energy converted to chemical energy [46].

$$\eta_{\text{solar-chemical}} = \frac{\dot{n}_{\text{prod}}\Delta H_{\text{prod}}}{\dot{Q}_{\text{solar}}} \tag{20}$$

where $\dot{n}_{\text{prod}}$ is the molar flow rate of syngas, ΔH_{prod} is the difference between the sum of enthalpies of all reaction products and that of all reactants.

Methane conversion is defined as the fraction of input methane converted to products.

$$X_{\text{CH}_4} = 1-\frac{\dot{n}_{\text{CH4,out}}}{\dot{n}_{\text{CH4,in}}} \tag{21}$$

where $\dot{n}_{\text{CH4,out}}$ is the molar flow rate of residual methane, and $\dot{n}_{\text{CH4,in}}$ is the molar flow rate of methane pumped into the reactor.

4. Results and discussion

For steam methane reforming, a steam-to-methane ratio of 2–3 is required in order to obtain a full conversion of methane and prevent coke formation [47]. Considering the potential impact of such ratio on performance metrics of the reactor, the steam-to-methane ratio is taken as 2, and carbon deposition is not considered for the simplicity of discussions. Kinetic and thermodynamic performances of the solar thermochemical reactor are studied.

4.1. Calibration of the numerical model

To validate the entire model with consideration of the kinetics of steam methane reforming reaction, an experimental study in a tubular reactor in Ref. [26] was used for comparison. We used the same model of the tubular reactor and boundary condition as those in Ref. [26]. The simulation results of methane conversion and hydrogen production compared with those obtained in the reference are shown in Fig. 3. It can be observed that the molar fractions of methane and hydrogen along the flow direction are in good agreement with the study in Ref. [26] and the maximum relative error is below 2.5%, which indicates that the numerical model is reliable.

4.2. Effect of cutoff wavelength coating

The cutoff wavelength coating is applied on both sides of the quartz window for minimizing the absorption of incident radiation by the window and reduction of secondary radiation loss from the interior of the reactor.

Fig. 4(a) shows the solar spectrum of AM 1.5 [48] and spectral energy distribution of thermal radiation from the reactor (850 °C). In Fig. 4(b), the ratio of cumulative solar energy integrated up to a given wavelength to the total solar energy input is a function of the wavelength, which increases much faster compared with that of the thermal radiation of a typical methane reforming reactor. Thus 80% of the outbound radiation energy from the reaction zone (850 °C) can be reflected back to the reactor at the cost of only 1% energy loss of incident sunlight by applying a coating with cutoff wavelength of 2400 nm. The reflected secondary radiation is absorbed by the reactants (H_2O and CH_4) which flow through the interlayer of the cone.

In order to analyze the effects of cutoff wavelength coating individually, we assume that the wall of the reforming reactor is well-insulated, which means that only thermal radiation loss through the aperture is considered. The actual heat dissipation model, including conduction, convection and radiation losses, is studied by combining the MCRT method and FEM in the following sections. Therefore, the

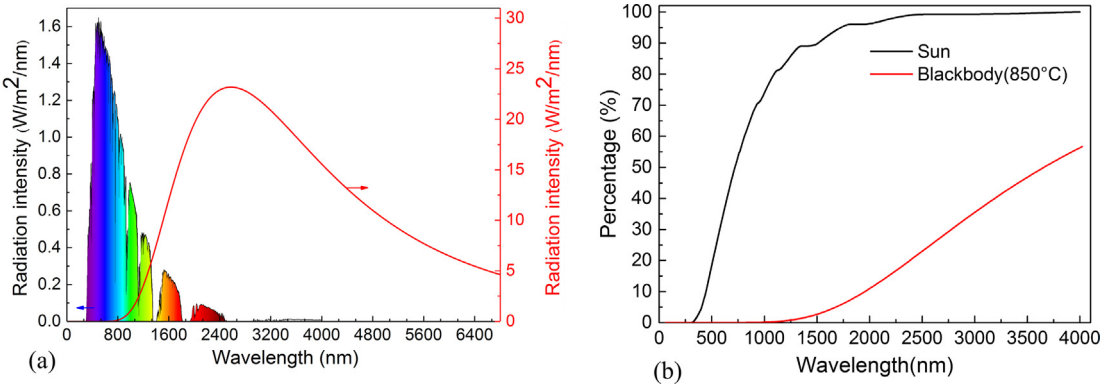

Fig. 4. (a) Solar spectrum at the earth's surface (AM 1.5) [48] (rainbow curve) and spectral energy distribution of blackbody radiation at 850 °C (red curve). (b) The ratio of cumulative energy percentage of the AM 1.5 solar irradiance and blackbody radiation at 850 °C as functions of wavelength.

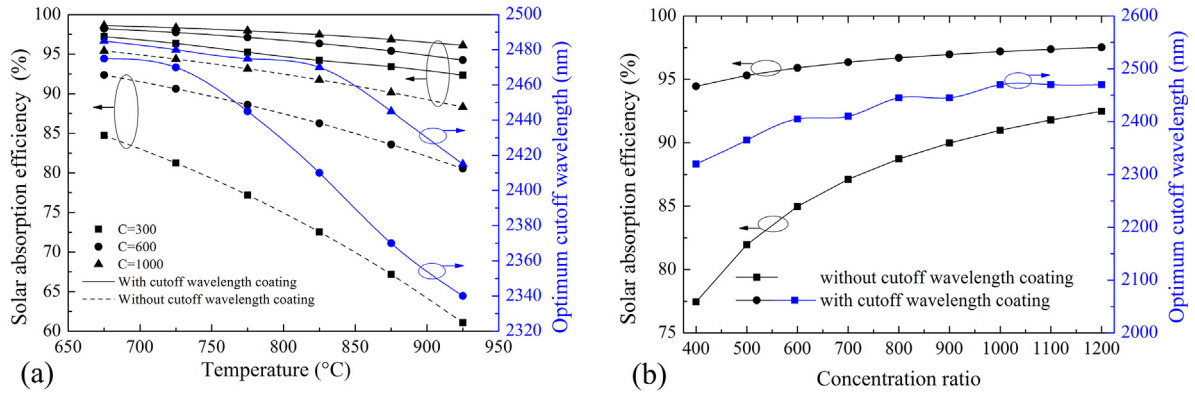

Fig. 5. Solar absorption efficiency and optimum cutoff wavelength of the reactor; (a) under different temperatures and concentration ratios; (b) under different concentration ratios at 850 °C.

solar absorption efficiency is defined as the fraction of solar energy captured by the reactor, given as:

$$\eta_{abs} = A - \frac{B\varepsilon\sigma T^4}{IC} \tag{22}$$

where A and B are transmissivities of the quartz window for incident sunlight and outgoing thermal radiation (assumed to be 1 without coating), respectively; ε is the emissivity of the reactor cavity (assumed to be 1), I is solar irradiance, taken as 1 kW·m^{-2} and C is solar concentration ratio. The cutoff wavelengths of the coating under different circumstances are optimized by maximizing η_{abs} using an in-house developed program. It can be found from Fig. 5(a) that the coating can significantly improve the efficiency of solar energy utilization. The solar absorption efficiency both with and without coating decreases as the temperature increases due to the fact that the energy flux of blackbody radiation is proportional to the fourth power of temperature. However, η_{abs} with cutoff wavelength coating drops at a much slower rate than that without coating because the coating can reflect most of thermal radiation back to the reactor, so that η_{abs} becomes much less sensitive to temperature after the coating is applied. The solar absorption efficiency with coating improves by more than 30 percentage points (from 61.07% to 91.89%) when temperature and concentration ratio are 925 °C and 300, respectively. The optimum cutoff wavelength decreases with the increase of temperature, because the peak wavelength of a blackbody radiation spectrum decreases with increasing temperature according to Wien's displacement law. Additionally, the effect of concentration ratio on solar absorption efficiency of the reactor at 850 °C is plotted in Fig. 5(b). It is observed that both optimum cutoff wavelength and solar absorption efficiency rise with the increase of concentration ratio. The curves have several inflection points, which result from the non-smoothness and discontinuities of the AM 1.5 solar spectrum (Fig. 4(a)). The solar absorption efficiency with coating is higher than that without coating, while their difference becomes smaller as concentration ratio increases, because the incoming solar energy flux increases with increasing concentration ratio while the radiation loss is constant (assuming the reactor temperature is fixed). The optimum cutoff wavelength increases with increasing concentration ratio for the same reason. Our analysis shows that cutoff wavelength coating can effectively improve solar absorption efficiency.

4.3. Effect of CPC

The CPC as a secondary concentrating device of sunlight can both improve the uniformity of solar energy distribution and reduce diameter of a cavity's aperture, which will alleviate radiation loss from the reactor to the ambient. The upper aperture diameter of CPC is determined by the size of focal spot of the dish collector, and the acceptance half angle is optimized by the MCRT method for getting more uniform flux distribution. The distribution of solar energy flux on the front and rear aperture planes of CPC is plotted in Fig. 6 based on parameters in Tables 1 and 2. It can be observed that solar energy flux distribution is symmetric in the circumferential direction, but the non-uniformity in the radial direction is quite significant. The peak and average fluxes without CPC are 4800 and 885 kW·m^{-2}, in contrast to 5436 and 1771 kW·m^{-2} with CPC, respectively. The peak-to-mean flux ratio decreases from 5.42 to 3.07 accordingly, signifying much enhanced uniformity of solar energy distribution, which is crucial to the reduction of temperature gradient and thermal stresses within the reactor. Meanwhile, the radius of aperture reduces from 25 mm to 17.6 mm, which is equivalent to a decrease in aperture area by 50% for further reduction of radiation loss.

4.4. System analysis results

The thermodynamic performance of solar steam methane reforming system is simulated by Aspen Plus [41]. Taking kinetics of the catalyst into account, the performance of the reactor is further studied by the FEM model. Under standard operating conditions, $\dot{Q}_{reactor}$ and $\dot{Q}_{preheater}$ are set to 2.0 kW and 0.45 kW, respectively, and the flow rate of methane is set to 0.005 mol/s with a steam-to-methane molar ratio of 2. Considering the reflectivity of solar dish collector (0.93) and transmittance of quartz window with cutoff wavelength coating (0.95), the actual energy entering the cavity is 1.77 kW. With the help of the coating, approximately 120 W of radiation power is reflected back to the reactor and absorbed by the reactants.

Figure 7 shows the temperature distribution in the reactor under standard operating conditions. The peak and average temperatures are approximately 850 °C and 800 °C with coating, while their values are about 830 °C and 790 °C without coating, respectively. Therefore, it proves that the coating can improve solar energy utilization efficiency and collection temperature. The temperature difference within the catalyst bed is not only influenced by the non-uniformity of solar energy flux distribution, but is also affected by the reaction rates. The non-uniformity of temperature of catalyst region is small, ascribing to the volumetric absorption of sunlight by RPC and assistance of CPC, which are both beneficial to the operation of the reactor. Additionally, the Al_2O_3 insulation wall significantly reduces convective heat loss, and the temperature of the external surface is ~45 °C during normal operations. However, the sensible heat carried away by both gas products and unreacted steam and methane accounts for 36.36% of total solar power input ($\dot{Q}_{solar}$), hence the temperature at the outlet of pipe is quite high. Consequently, attention must be paid to heat recovery from the exhaust for reducing energy loss and further improving the performance of reactor.

The molar fraction of reactants in the reaction zone is shown in Fig. 8 under standard operating conditions. Methane and steam are

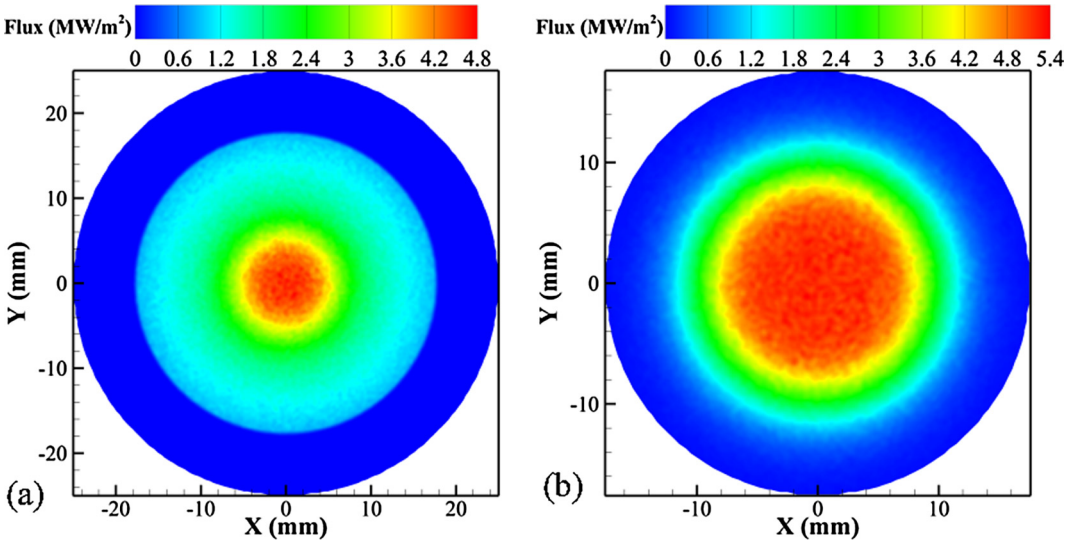

Fig. 6. Energy flux maps of the CPC: (a) front aperture plane; (b) rear aperture plane.

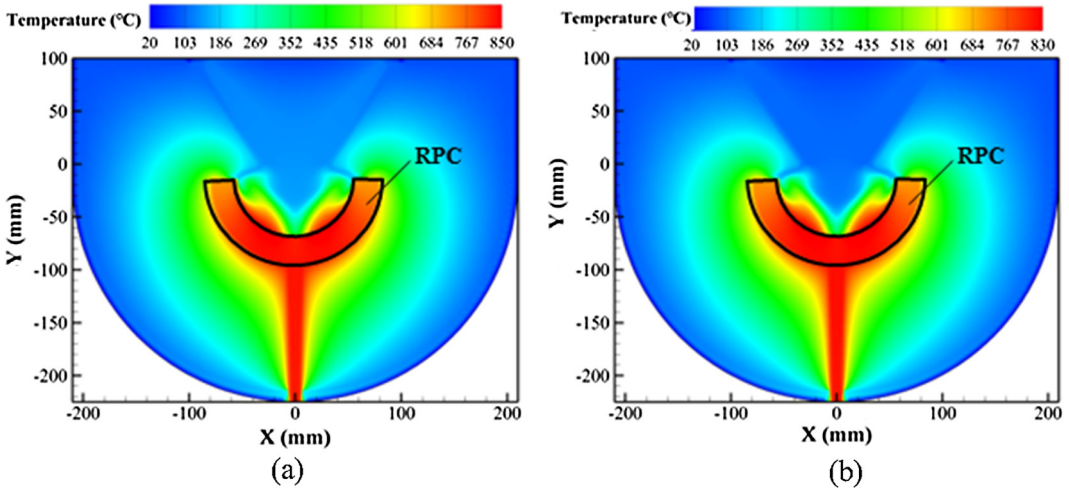

Fig. 7. Temperature distribution in the reactor under 1.77 kW solar power input; pressure is 1 atm and the flow rate of methane is 0.005 mol/s, with a steam-to-methane molar ratio of 2: (a) with coating; (b) without coating.

injected into the reactor through the interlayer of cone and the reforming reaction takes place within the catalyst bed region. The reaction products (H_2, CO and CO_2) exhibit similar distributions but different ranges of molar fraction: H_2 has the highest share while CO_2 has the lowest. Besides, the gas residence time near the outlet is considerably shorter, since convective transport of gas species is much stronger than that in other regions of the catalyst bed. Therefore, the molar fraction of gas products near the outlet is lower than that in other regions of the catalyst bed.

Figure 9 shows the performance metrics of the reactor (methane conversion, thermal efficiency and solar-to-chemical efficiency) as functions of steam-to-methane ratio at 1.77 kW solar power input and a constant total molar flow rate of reactants feed. It can be seen that $\eta_{thermal}$ is almost constant at 76% because the heat loss is significantly reduced (the coating reduces ~80% thermal radiation loss and the Al_2O_3 insulation wall greatly reduces convective heat loss), while $\eta_{solar-chemical}$ decreases from 45.6% to 22.8% as steam-to-methane ration increases from 1.0 to 5.0 (without any heat recovery), shown in Fig. 9(b). Since the total flow rate of reactants is set to 0.015 mol/s, the flow rate of methane decreases as steam-to-methane molar ratio increases, which explains the decrease of gas products. Meanwhile, the flow rate (and thus molar ratio) of steam increases, thereby increasing the energy cost for heating and vaporizing water, so that the solar-to-chemical efficiency decreases, as shown in Fig. 9(b). Meanwhile, the power absorbed by chemical reactions decreases, resulting in an increase in reactor temperature. Moreover, it shall be noted that the endothermic steam methane reforming reaction shifts in the direction of lager steam-to-methane ratios and higher temperatures in favor of higher methane conversion. Hence, suitable steam-to-methane ratio is important to obtain high methane conversion and $\eta_{solar-chemical}$. Considering the finite kinetics of catalyst, methane conversion is lower than the theoretical value calculated by Aspen Plus [41], and the difference between them decreases with increasing temperature, the reason of which lies in the exponential relationship between reaction rates (Table 3) and temperature for methane reforming, thus the actual chemical reaction performance gradually approaches its thermodynamic limit as temperature rises. We also find that $\eta_{solar-chemical}$ rises by approximately 19.5 percentage points when 90% heat recovery is applied to preheat reactants, so that $\eta_{solar-chemical}$ could reach 59.16% under standard operating conditions with 90% heat recovery, which is much higher than other solar thermochemical systems (such as water/carbon dioxide splitting) due to the relative ease of fossil fuel conversion.

Performance of the reactor with constant inputs of methane

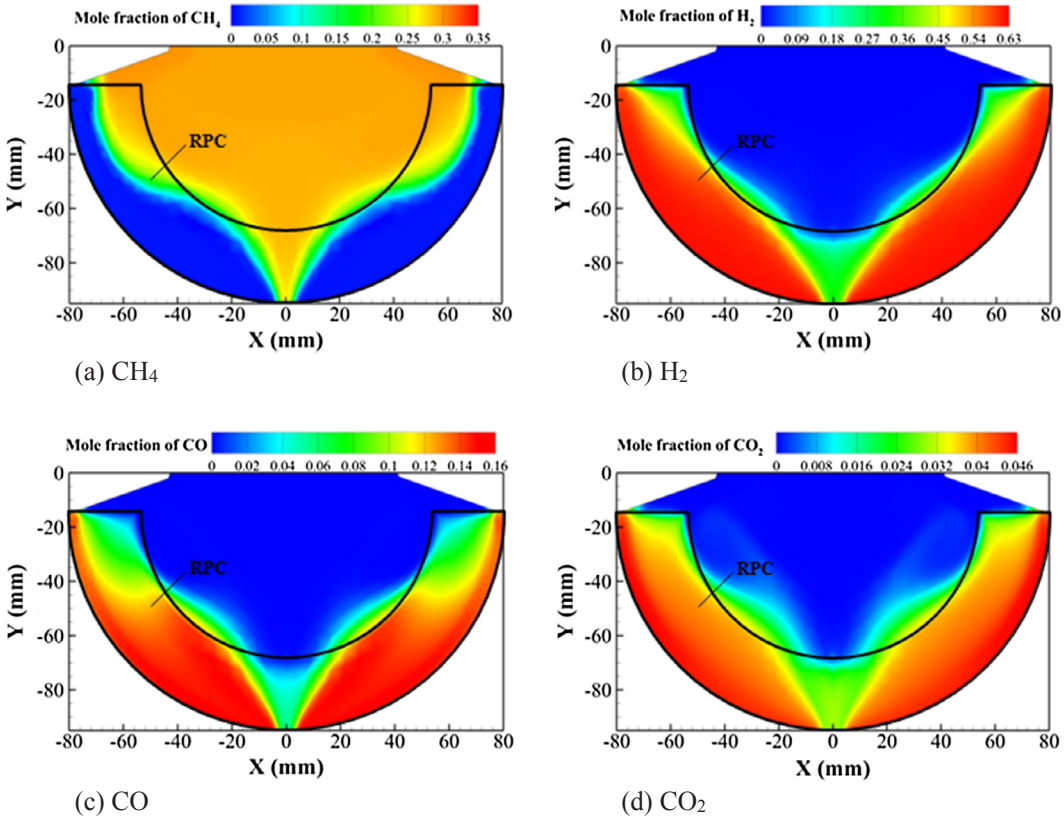

Fig. 8. Molar fraction distribution of reactants in the reaction zone under solar input power of 1.77 kW, total pressure of 1 atm, methane flow rate of 0.005 mol/s, and steam-to-methane molar ratio of 2. The semi-annular region delineated by the black lines demarcates the reaction zone, i.e. location of the catalyst bed.

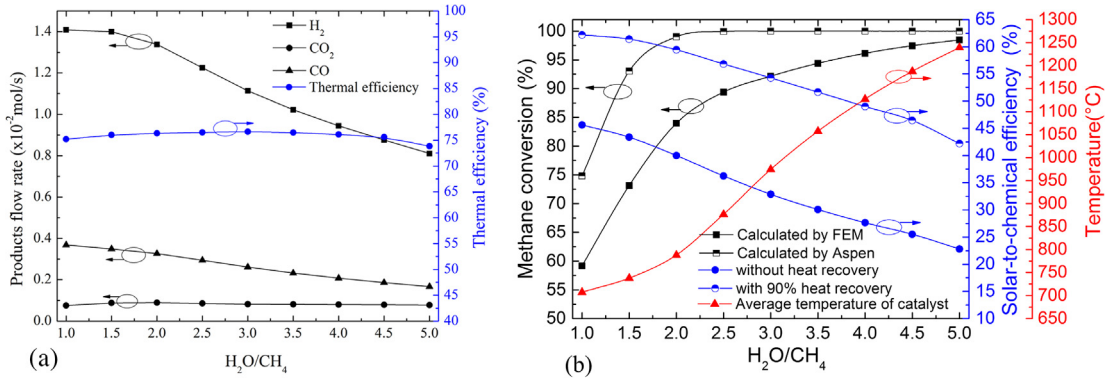

Fig. 9. Performances of the reactor as functions of steam-to-methane ratio at 1.77 kW of total solar power input and constant total molar flow rate of input reactants. (a) molar flow rate of products and thermal efficiency of the reactor, (b) methane conversion and solar-to-chemical efficiency of the reactor.

(0.005 mol/s) and water (0.010 mol/s) and a varying input of solar energy is shown in Fig. 10. The thermal efficiency exhibits a similar trend to that in Fig. 9, which is almost constant at 75.5%, but the flow rate of gas products is reversed, which increases with the increment of solar power input. Due to a higher solar power input into the reactor cavity, temperature of the catalyst bed and the reaction rates are both enhanced. Consequently, methane conversion obviously increases with the increment of input solar power. Despite an increasing solar power input, the methane conversion rate also enhances at roughly the same speed, so that $\eta_{solar-chemical}$ is relatively constant, which means that the chemical energy storage capacity can be relatively easily scaled up without sacrificing efficiency. The increase in solar power input drives up reactor temperature monotonically, so that not only the practical (i.e. by FEM) and theoretical (i.e. by Aspen Plus) conversion rates of methane enhance in a similar manner, but the former also asymptotically approaches the latter (i.e. the thermodynamic conversion limits) as reaction kinetics plays an increasingly important role. The resemblance becomes apparent when Fig. 10(b) is compared with Fig. 9(b). Also, the improvement of solar-to-chemical efficiency resulting from heat recovery shows a similar trend between the two figures, for the simple reason that heat recovery dramatically reduces the energy cost for preheating reactants.

In sum, temperature distribution within the catalyst bed is relatively uniform with CPC and RPC structure, and notably the difference between the highest and average temperature is ~50 °C. For an input solar power of 1.77 kW, the temperature of the catalyst bed can reach ~850 °C and $\eta_{solar-chemical}$ is 39.98% and 59.16% without and with 90% heat recovery, respectively. With the help of the cutoff wavelength coating, the peak and average temperature can increase by 20 °C and 10 °C, respectively, and ~120 W of radiation loss is saved, which accounts for 5% of total energy input. Although thermal insulation works fine, heat loss from the reactor to the ambient in the form of thermal

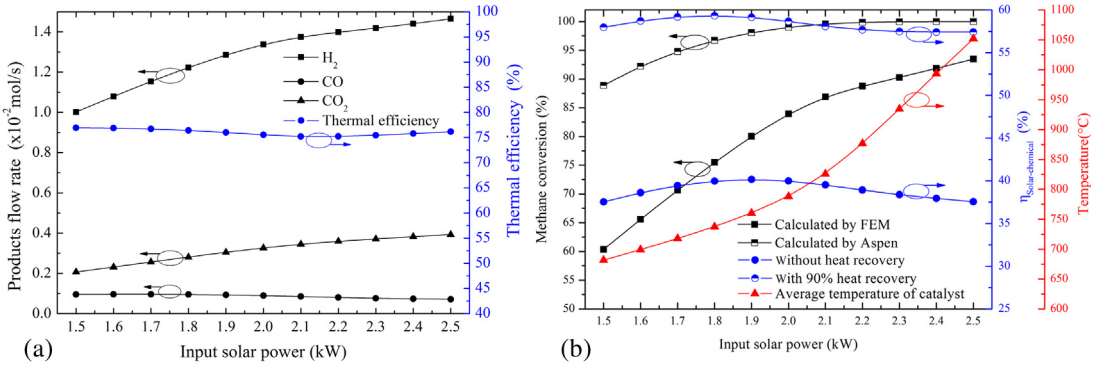

Fig. 10. Performances of the reactor as functions of solar power input at a constant molar flow rate (0.015 mol/s) of input reactants. (a) molar flow rate of products and thermal efficiency of the reactor, (b) methane conversion and solar-to-chemical efficiency of the reactor.

conduction and convection still accounts for 15% of the total input solar power. Therefore, better insulation materials and designs are needed to further reduce heat losses.

5. Conclusions

A new solar methane reforming reactor design featuring cutoff wavelength window and compound parabolic concentrator (CPC) has been conceptually proposed and analyzed with reticulated porous ceramics (RPC) structure of Ni/CeO_2-ZrO_2 used as the catalyst. Performance of the reactor is numerically investigated by combining finite-element method (FEM) and Monte-Carlo ray-tracing (MCRT) method. Results show that the solar-to-chemical efficiency, after taking optical loss, kinetics of catalyst and all heat losses into account, reaches up to 39.98% and 59.16% at a typical operating temperature of 850 °C and pressure of 1 atm without and with 90% heat recovery from the exhaust, respectively. Meanwhile, the thermal efficiency is 76.02% and methane conversion is 83.95%. Compared with conventional reactor designs, cutoff wavelength coating and CPC are the key measures that effectively reduce 80% of radiation loss from the reactor to the ambient, which could save 5% of total energy input. Additionally, the CPC and RPC structure can also enhance uniformity of solar energy distribution within the catalyst with the highest and average temperature being 850 °C and 800 °C, respectively, so as to minimize temperature gradient and thermal stress of the reactor.

We also analyzed the influences of solar power input and steam-to-methane ratio on efficiencies and methane conversion. Results show that greater steam-to-methane ratios favor methane conversion but adversely affects solar-to-chemical efficiency. Within a relatively wide range of solar power input conditions, methane conversion rate improves directly proportional to the input solar power, but the solar-to-chemical efficiency remains relatively stable. Accordingly, appropriate steam-to-methane ratio (e.g. 2) and solar power input are necessary for optimum performances of solar methane reforming reactors.

The reactor design proposed in this study is capable of achieving enhanced solar-to-chemical efficiency for solar methane reforming, which might considerably improve the efficiency of solar energy utilization and reduce investment of solar thermal and thermochemical technologies.

Acknowledgment

This study was supported by the National Natural Science Foundation under award number 51676189, the Chinese Academy of Sciences International Collaboration Key Program under award number 182211KYSB20160043, and the Chinese Academy of Sciences Frontier Science Key Research Project under award number QYZDYSSW-JSC036.

References

[1] Crabtree George W, Lewis Nathan S. Solar energy conversion. Phys Today 2007;60:37–42. http://dx.doi.org/10.1111/j.1365-3040.2009.02017.x.
[2] Lu J, Chen Y, Ding J, Wang W. High temperature energy storage performances of methane reforming with carbon dioxide in a tubular packed reactor. Appl Energy 2016;162:1473–82. http://dx.doi.org/10.1016/j.apenergy.2015.03.140.
[3] Steinfeld A, Palumbo R. Solar thermochemical process technology. Encycl Phys Sci Technol 2001;15:237–56. http://dx.doi.org/10.1016/B0-12-227410-5/00698-0.
[4] Cinti G, Baldinelli A, Di Michele A, Desideri U. Integration of solid oxide electrolyzer and Fischer-Tropsch: a sustainable pathway for synthetic fuel. Appl Energy 2016;162:308–20. http://dx.doi.org/10.1016/j.apenergy.2015.10.053.
[5] Said SAM, Waseeuddin M, Simakov DSA. A review on solar reforming systems. Renew Sustain Energy Rev 2016;59:149–59. http://dx.doi.org/10.1016/j.rser.2015.12.072.
[6] Gokon N, Osawa Y, Nakazawa D, Kodama T. Kinetics of CO_2 reforming of methane by catalytically activated metallic foam absorber for solar receiver-reactors. Int J Hydrogen Energy 2009;34:1787–800. http://dx.doi.org/10.1016/j.ijhydene.2008.12.018.
[7] Barroso-Quiroga MM, Castro-Luna AE. Catalytic activity and effect of modifiers on Ni-based catalysts for the dry reforming of methane. Int J Hydrogen Energy 2010;35:6052–6. http://dx.doi.org/10.1016/j.ijhydene.2009.12.073.
[8] Nagaoka K, Seshan K, Aika KI, Lercherz JA. Carbon deposition during carbon dioxide reforming of methane – comparison between Pt/$Al_2O_3$and Pt/ZrO_2. J Catal 2001;197:34–42. http://dx.doi.org/10.1006/jcat.2000.3062.
[9] Abbas HF, Daud WMAW. Hydrogen production by methane decomposition: a review. Int J Hydrogen Energy 2010;35(3):1160–90. http://dx.doi.org/10.1016/j.ijhydene.2009.11.036.
[10] Sheu EJ, Ghoniem AF. Redox reforming based, integrated solar-natural gas plants: reforming and thermodynamic cycle efficiency. Int J Hydrogen Energy 2014;39:14817–33. http://dx.doi.org/10.1016/j.ijhydene.2014.07.086.
[11] Jang W-J, Jeong D-W, Shim J-O, Kim H-M, Roh H-S, Son IH, et al. Combined steam and carbon dioxide reforming of methane and side reactions: thermodynamic equilibrium analysis and experimental application. Appl Energy 2016;173:80–91. http://dx.doi.org/10.1016/j.apenergy.2016.04.006.
[12] Simakov DSA, Wright MM, Ahmed S, Mokheimer EMA, Roman-Leshkov Y, Romn-Leshkov Y. Solar thermal catalytic reforming of natural gas: a review on chemistry, catalysis and system design. Catal Sci Technol 2015;5:1991–2016. http://dx.doi.org/10.1039/C4CY01333F.
[13] Hafizi A, Rahimpour MR, Hassanajili S. Hydrogen production via chemical looping steam methane reforming process: effect of cerium and calcium promoters on the performance of Fe_2O_3/Al_2O_3 oxygen carrier. Appl Energy 2016;165:685–94. http://dx.doi.org/10.1016/j.apenergy.2015.12.100.
[14] Zhao K, He F, Huang Z, Wei G, Zheng A, Li H, et al. Perovskite-type oxides $LaFe_{1-x}Co_xO_3$ for chemical looping steam methane reforming to syngas and hydrogen co-production. Appl Energy 2016;168:193–203. http://dx.doi.org/10.1016/j.apenergy.2016.01.052.
[15] Sheu EJ, Ghoniem AF. Receiver reactor concept and model development for a solar steam redox reformer. Sol Energy 2016;125:339–59. http://dx.doi.org/10.1016/j.solener.2015.12.024.
[16] Zheng R, Diver R, Caldwell D, Fritz B, Cameron R, Humble P, et al. Integrated solar thermochemical reaction system for steam methane reforming. Energy Procedia 2015;69:1192–200. http://dx.doi.org/10.1016/j.egypro.2015.03.204.
[17] Dong W-S, Roh H-S, Jun K-W, Park S-E, Oh Y-S. Methane reforming over Ni/Ce-ZrO_2 catalysts: effect of nickel content. Appl Catal A Gen 2002;226:63–72. http://dx.doi.org/10.1016/S0926-860X(01)00883-3.
[18] Hou K, Hughes R. The kinetics of methane steam reforming over a Ni/α-Al_2O_3 catalyst. Chem Eng J 2001;82:311–28.
[19] Spi I, Tyner CE, Langnickel U. Applications of solar reforming technology. Tech Rep Sandia National Laboratories 1993.
[20] Klein HH, Karni J, Rubin R. Dry methane reforming without a metal catalyst in a directly irradiated solar particle reactor. J Sol Energy Eng 2009;131:021001. http://dx.doi.org/10.1115/1.3090823.

[21] Anikeev VI, Bobrin AS, Ortner J, Schmidt S, Funken KH, Kuzin NA. Catalytic thermochemical reactor/receiver for solar reforming of natural gas: design and performance. Sol Energy 1998;63:97–104. http://dx.doi.org/10.1016/S0038-092X(98)00050-4.
[22] Tanashev YY, Fedoseev VI, Aristov YI. High-temperature catalysis driven by the direct action of concentrated light or a high-density electron beam. Catal Today 1997;39:251–60.
[23] Wörner A, Tamme R. CO_2 reforming of methane in a solar driven volumetric receiver–reactor. Catal Today 1998;46:165–74. http://dx.doi.org/10.1016/S0920-5861(98)00338-1.
[24] Yuan Q, Ding J, Lu J, Yu T, Wang W. Heat Transfer and energy storage performance of methane reforming with carbon dioxide in semi-cavity reactor. Procedia Eng 2016;157:365–73. http://dx.doi.org/10.1016/j.proeng.2016.08.378.
[25] Yu T, Yuan Q, Lu J, Ding J, Lu Y. Thermochemical storage performances of methane reforming with carbon dioxide in tubular and semi-cavity reactors heated by a solar dish system. Appl Energy 2015;185:1994–2004. http://dx.doi.org/10.1016/j.apenergy.2015.10.131.
[26] Yuan Q, Gu R, Ding J, Lu J. Heat transfer and energy storage performance of steam methane reforming in a tubular reactor. Appl Therm Eng 2017;125:633–43. http://dx.doi.org/10.1016/J.APPLTHERMALENG.2017.06.044.
[27] Rieks M, Bellinghausen R, Kockmann N, Mleczko L. Experimental study of methane dry reforming in an electrically heated reactor. Int J Hydrogen Energy 2015;40:15940–51. http://dx.doi.org/10.1016/j.ijhydene.2015.09.113.
[28] Mozdzierz M, Brus G, Sciazko A, Komatsu Y, Kimijima S, Szmyd JS. Towards a thermal optimization of a methane/steam reforming reactor. Flow, Turbul Combust 2016;97:171–89. http://dx.doi.org/10.1007/s10494-015-9693-2.
[29] Pennemann H, Bellinghausen R, Westermann T, Mleczko L. Reforming of methane in a multistage microstructured reactor. Chem Eng Technol 2015;38:1883–93. http://dx.doi.org/10.1002/ceat.201500193.
[30] Gordon JM, Kashin P, Rabl A. Nonimaging reflectors for efficient uniform illumination. Appl Opt 1992;31:6027–35. http://dx.doi.org/10.1364/AO.31.006027.
[31] Welford WT, Winston R. High collection nonimaging optics. San Diego: Academic Press; 1989.
[32] Chueh WC, Falter C, Abbott M, Scipio D, Furler P, Haile SM, et al. High-flux solar-driven thermochemical dissociation of CO_2 and H_2O using nonstoichiometric ceria. Science 2010;330:1797–801. http://dx.doi.org/10.1126/science.1197834.
[33] Furler P, Scheffe JR, Marxer D, Steinfeld A. Solar thermochemical CO_2 splitting using a reticulated porous ceria redox system. Energy Fuels 2012;26:7051–9. http://dx.doi.org/10.1021/ef3013757.
[34] Hamberg I, Granqvist CG. Evaporated Sn-doped In2O3 films: Basic optical properties and applications to energy-efficient windows. J Appl Phys 1986;60. http://doi.org/10.1063/1.337534.
[35] Dudley VE, Kolb GJ, Mahoney AR, Mancini TR, Matthews CW, Sloan M, et al. SEGS LS2 solar collector-test results. SAN94-1884; 1994.
[36] Röger M, Rickers C, Uhlig R, Neumann F, Polenzky C. Infrared-reflective coating on fused silica for a solar high-temperature receiver. J Sol Energy Eng 2009;131:021004. http://dx.doi.org/10.1115/1.3097270.
[37] Meier A, Steinfeld A. Solar thermochemical production of fuels. Adv Sci Technol 2010;74:303–12. http://dx.doi.org/10.4028/www.scientific.net/AST.74.303.
[38] Furler P, Steinfeld A. Heat transfer and fluid flow analysis of a 4kW solar thermochemical reactor for ceria redox cycling. Chem Eng Sci 2015;137:373–83. http://dx.doi.org/10.1016/j.ces.2015.05.056.
[39] Marxer D, Furler P, Takacs M, Steinfeld A. Solar thermochemical splitting of CO_2 into separate streams of CO and O_2 with high selectivity, stability, conversion, and efficiency. Energy Environ Sci 2017. http://dx.doi.org/10.1039/C6EE03776C.
[40] Roses L, Manzolini G, Campanari S. CFD simulation of Pd-based membrane reformer when thermally coupled within a fuel cell micro-CHP system. Int J Hydrogen Energy 2010;35:12668–79. http://dx.doi.org/10.1016/j.ijhydene.2010.07.080.
[41] Aspen Plus®. Aspen technology, Inc., version 8.2, http://www.aspentech.com/.
[42] Jin J, Ling Y, Hao Y. Similarity analysis of parabolic-trough solar collectors. Appl Energy 2017;204:958–65. http://dx.doi.org/10.1016/j.apenergy.2017.04.065.
[43] Hs F. Elements of chemical reaction engineering. New Jersey: Prentice Hall; 1999.
[44] Fuller EN, Schettler PD, Giddings JC. A new method for prediction of binary gas-phase diffusion coefficients. Ind Eng Chem 1966;58:18–27. http://dx.doi.org/10.1021/ie50677a007.
[45] Xu JG, Froment GF. Methane Steam Reforming, Methanation and Water-Gas Shift. 1. Intrinsic Kinetics. Aiche J 1989;35:88–96. http://dx.doi.org/10.1002/aic.690350109.
[46] Sheu EJ, Mokheimer EMA, Ghoniem AF. A review of solar methane reforming systems. Int J Hydrogen Energy 2015;40:12929–55. http://dx.doi.org/10.1016/j.ijhydene.2015.08.005.
[47] Liu JA. Kinetics, catalysis and mechanism of methane steam reforming [Masters thesis]. Worcester Polytechnic Institute; 2006.
[48] Gueymard CA, Myers D, Emery K. Proposed reference irradiance spectra for solar energy systems testing. Sol Energy 2002;73:443–67. http://dx.doi.org/10.1016/S0038-092X(03)00005-7.